

Non-Isothermal Modeling of Planar Solid Oxide Fuel Cell

Mohammed Ali Farzad | Hasan Hassanzadeh*

Department of Mechanical Engineering, University of Birjand, Birjand Iran

* Corresponding author, Email: h.hassanzadeh@birjand.ac.ir

Article Information

Article Type

RESEARCH ARTICLE

Article History

RECEIVED: 27 Oct 2024

REVISED: 11 Dec 2024

ACCEPTED: 15 Feb 2025

PUBLISHED ONLINE: 03 Mar 2025

Keywords

SOFC

Planar

Variable properties

Non-isothermal

Abstract

A Solid Oxide Fuel Cell (SOFC) with internal reformation and a parallel flow configuration is modeled. The solution domain of the model is divided into four sections: the fuel channel, air channel, bipolar plates, and the cell core (PEN), which comprises the anode and cathode electrodes as well as the electrolyte. The conservation equations for mass, momentum, and energy, along with an electrochemical model, are solved in a one-dimensional steady-state framework using gPROMS software. The model's results have been validated against data available in published literature. First, the equations were solved using both variable properties (temperature-dependent) and constant properties, and the results were compared. The results show that the impact of temperature on properties within the performance range of the SOFC is negligible. Therefore, the results were obtained using constant properties, which reduced the program execution time by 16.7%. Secondly, to further reduce the program execution time, the various terms in the governing equations were analyzed based on their order of magnitude. Terms with lower significance were eliminated from the equations. The results of the simplified equations were then compared to those obtained from the original equations, ensuring consistency and accuracy. The effects of parameters such as the fuel pre-reforming percentage, inlet temperature, and fuel utilization factor on fuel cell performance have been investigated. The results show that the fuel utilization factor has a direct relationship with the temperature gradient and an inverse relationship with the power output and efficiency of the fuel cell. Additionally, increasing the excess air leads to a reduction in the operational performance of the cell.

Cite this article: Farzad, M. A., Hassanzadeh, H. (2025). Non-Isothermal Modeling of Planar Solid Oxide Fuel Cell. DOI: [10.22104/hfe.2024.7092.1326](https://doi.org/10.22104/hfe.2024.7092.1326)



© The Author(s).

DOI: [10.22104/hfe.2024.7092.1326](https://doi.org/10.22104/hfe.2024.7092.1326)

Publisher: Iranian Research Organization for Science and Technology (IROST)

1 Introduction

The growing energy demand, heightened public awareness, stringent environmental protection regulations, and rising fossil fuel prices have driven efforts to explore alternative and renewable energy sources, as well as develop more efficient energy conversion systems. Small-scale power generation systems, such as wind turbines, photovoltaic systems, microturbines, and fuel cells, can play an important role in meeting the demand for cleaner energy sources. These systems are typically located near the point of consumption and can function as part of a distributed power generation network, enhancing energy efficiency and reducing transmission losses. Among the various small-scale power generation systems, fuel cells have attracted significant attention due to their ability to generate a portion of the electricity needed by consumers. This capability reduces reliance on electricity purchases from power generation companies, offering both economic and environmental benefits. Furthermore, fuel cells can function as cogeneration systems, simultaneously producing electricity and utilizing excess heat to provide heating and hot water for residential use. This feature is generally not feasible for large power plants, except in cases where they are located in close proximity to the point of consumption [1].

Solid oxide fuel cells offer several advantages, including a high operating temperature of 800-1000 °C, fuel flexibility, reduced emissions of NO_x and SO_x compared to thermal engines, resistance to sulfur, insensitivity to carbon monoxide (CO), and the ability to function without the need for expensive catalysts. Their high efficiency and significant potential for cogeneration make them particularly valuable for household and power plant applications [2–4]. However, they also have notable drawbacks, such as the high cost of materials typically expensive ceramics and alloys and the lengthy setup time required for operation. Solid oxide fuel cells are typically designed in two geometries: planar and tubular. The tubular fuel cell offers advantages such as lower thermal stress and better sealing compared to the planar type. However, the planar fuel cell has a higher power density and lower manufacturing cost, making it more cost-effective in certain applications. In addition, in the planar-type fuel cell, as shown in the figure, the flow path selection in the fuel and oxidizer distributor plates can be easily implemented. The arrangement of the flow paths in the distributor plates – whether in the same direction, different directions, or cross-flow – has a significant impact on both the temperature distribution and current density distribution within the fuel cell.

Given these advantages, this research focuses on the investigation of the planar-type fuel cell [5]. A solid oxide fuel cell, as shown in Figure 1, is made of two porous electrodes that are separated from each other by a solid, non-porous, ion-conducting electrolyte. According to this figure, the oxygen entering the cathode electrode reacts with the transferred electrons from the anode electrode, and oxide ions (O²⁻) are formed.

After that, the oxide ions pass through the solid electrolyte and combine with H₂ molecules in the anode catalyst to form water and electrons, thus completing the circuit. Reaction equations in the cathode and anode electrodes for H₂ are as follows:

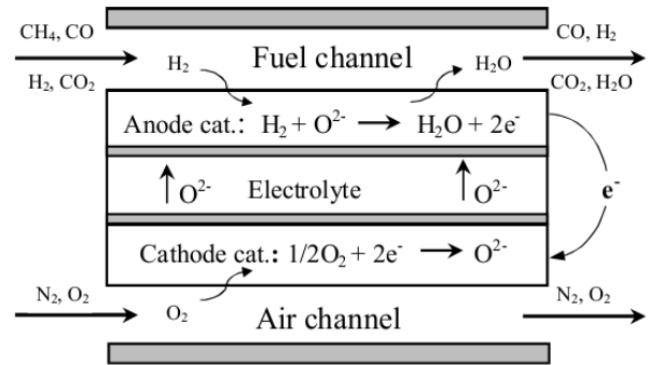


Fig. 1. Solid oxide fuel cell schematic.

Hydrogen is considered the ideal fuel for all types of fuel cells because of its simple reaction kinetics [6]. However, pure hydrogen does not naturally exist and is typically found in combination with other elements, necessitating its extraction through various processes. One common method for hydrogen production is the electrolysis of water, often powered by renewable energy sources. Another method is the reformation of simple hydrocarbons such as methane (at high temperatures) and methanol. During the fuel reformation process, in addition to the hydrogen oxidation reaction in the anode catalyst, methane reforming reactions and the water-gas shift reaction also occur in the fuel channel.

Due to the complexity of fuel cell processes and the challenge of obtaining the necessary experimental data, modeling becomes essential. These models can offer insights into various parameters such as voltage, current density, temperature, velocity, and species concentration as functions of position and time for different fuel cell configurations under varying operating conditions. Fuel cell models can be zero-dimensional, one-dimensional, or multi-dimensional in complexity. However, most models used for stack modeling of fuel cell

systems are simplified to reduce computational complexity and program execution time. For this reason, a one-dimensional model has been employed in this study.

Several studies have been carried out on single solid oxide fuel cell modeling over the past few decades, some of which are referenced here. Aguiar et al. [7] modeled a single planar fuel cell in one dimension under steady-state conditions. They solved the species and energy conservation equations but neglected the effects of pressure and velocity variations along the channel. In this study, Validation was performed only for the electrochemical part of the fuel cell, using four power density data points. Aguiar et al. [7] also investigated the effect of the direction of fuel and air flows (parallel vs. non-parallel) and found that, under the same conditions, non-parallel flow produced higher voltage, power density, and efficiency compared to parallel flow. However, in the non-parallel flow configuration, the average temperature of the cell was higher, and the temperature gradient was more intense, which they identified as a potential drawback of this configuration. In a subsequent study, these researchers [8] examined the effect of varying the load (current) on a fuel cell with parallel current. Ayora et al. [9] expanded on the previous model by incorporating the effects of local changes in thermophysical properties such as temperature, pressure, and velocity. They studied their impact on both the static and dynamic behavior of the fuel cell. They found that although the local temperature differences between the two models were less than 7K and the efficiency differences were below 1%, the deviation increased as the current density rose.

Rokhnagel et al. [10], using the MP-SOFC code in a three-dimensional geometry, explored the effect of fuel modification at the anode on the efficiency of the fuel cell. Their study provided valuable insights into how fuel composition changes could influence overall fuel cell performance. Their results show that to minimize thermal stress in the fuel cell anode in both cross-flow and asymmetrical flow geometries, the fuel pre-reformation (methane) should be 50-60%. Petersen et al. [11] presented a steady-state, zero-dimensional model of a planar solid oxide fuel cell with parallel flow using DNA software. They also investigated the internal fuel cell reactions, including hydrogen electrooxidation, methane reforming, and the water-gas shift reaction. The equilibrium reaction assumption was applied to model both the methane reforming and water-gas shift reactions. Finally, these researchers first calibrated and then validated the electrochemical part of their model using experimental results.

Cheddie and Munroe [12] presented a one-dimensional fuel cell model without internal fuel ref-

ormation for real-time simulation using Simulink software. To reduce calculation time and avoid the iterative solution process, they employed simplifying assumptions, including thermal integrity of the fuel and air channels, bipolar plates, anode, cathode, and electrolyte integrity, uniform current distribution throughout the fuel cell, and calculation of voltage losses under average cell conditions. These researchers finally validated the results with a complete one-dimensional model. They noted that increasing the width of the channels significantly reduces pressure drop and, consequently, the pump work.

Xie et al. [13] presented a simple zero-dimensional model to investigate solid oxide fuel cell control methods. They emphasized that studying the control of fuel cell behavior requires a simple model with minimal differential quantities. Therefore, they first developed a zero-dimensional model of the fuel cell, then simplified the mass conservation equations using the minimum Gibbs free energy method, and compared the results of both static and dynamic models. Chaisanticulat et al. [14] investigated the dynamic behavior of a planar solid oxide fuel cell with an anode support using COMSOL software. In this model, the flow is non-aligned, and hydrogen is used as the fuel. The study analyzed the fuel cell's response to a single-step change in the input gas concentration and flow.

Kang et al. [15] presented a simplified one-dimensional model of a planar solid oxide fuel cell with internal fuel reformation. Their simplifications included assuming temperature uniformity across the entire width of the fuel cell and a uniform distribution of current density along the length of the cell. This approach thermally modeled the entire cell in just its length direction. This modeling was conducted in MATLAB software, and its static and dynamic behavior was compared with both a one-dimensional and a zero-dimensional model. The researchers noted that their model offers comparable accuracy to the one-dimensional model, but with significantly reduced solution time. As a result, this model has been proposed for modeling fuel cell systems.

Salugni and Colonna [16] implemented the model by Aguiar et al. [17] using Modelica and validated their results by comparing them with previous research findings. Vakofsti et al. [18], considering the species conservation equation, the Navier-Stokes equation, and the energy conservation equation (without accounting for radiation), modeled a solid oxide fuel cell with internal fuel reformation in three dimensions using ACE-CFD+ software. The electrochemical model in this study is not complete and is limited to investigating the Butler-Volmer equation. These researchers examined the impact of temperature variations along the

length of the cell on other variables. They concluded that temperature changes along the length of the cell have a minimal effect on the velocity distribution in the channels but have a more significant impact on the species distribution. Soter et al [19] presented a zero-dimensional model of a SOFC with natural gas and internal reformation. They investigated the effects of various parameters on activation loss, ohmic loss, and concentration loss. Finally, the calculated fuel cell voltage values were compared with experimental data from Siemens Company, which used tubular geometry.

Maro et al. [20] developed a finite element numerical solution algorithm for three-dimensional modeling of a planar solid oxide fuel cell and validated their results with previous studies. Zabihian and Fang [21] compared and classified various methods of modeling composite systems based on solid oxide fuel cells in their study. The classification criteria included the stack modeling method of the fuel cell, combined cycles based on SOFCs, different system configurations, parametric and economic evaluations, fuel variety, and carbon dioxide production rate. In their article, they emphasized the lack of laboratory data for validating mathematical models and stated that, out of the 39 selected references, only two had been validated. In Iran, some studies have been carried out on SOFCs.

Ghanbari and Ghofrani [22] developed a zero-dimensional model of a planar solid oxide fuel cell using hydrogen as fuel. One of the key strengths of this research is its comprehensive electrochemical model. Similarly, Pirkandi et al. [23] modeled a hybrid system combining tubular solid oxide fuel cells and a micro-turbine, also using a zero-dimensional model. In their model, the fuel reforming reaction is considered as equilibrium, and a simplified version of the Butler-Volmer equation is used to model the reactions. Additionally, Kazempour et al. [24] conducted similar work, modeling a hybrid fuel cell and gas turbine system. Bozorgmehri et al. [25] conducted an experimental investigation into the microstructures of a single solid oxide fuel cell and derived valuable experimental constants. They then presented a zero-dimensional model and validated it against their experimental results. Among the published one-dimensional studies, the most comprehensive research is that of Kazempour and Ommi [26]. Their study presents a one-dimensional model that shares some similarities with the present study, as well as key differences. The geometry, boundary conditions, electrochemical model, and radiation model are similar in both studies, and both are steady-state models. However, they differ in the form of the governing equations, the method for calculating pressure drop, thermophysical properties, solution methods, and validation approaches.

Moulai et al. [27] presented a three-dimensional model of a programmable SOFC, which provides valuable insights in the field of SOFCs. However, the complexity of this model makes it less efficient for investigating simultaneous production systems with multiple components, as it significantly increases the calculation time. As can be seen, numerous one-, two- and three-dimensional studies have been conducted on fuel cells. In these articles, some have been validated with numerical data, while only a few have used experimental results for validation. Due to the complexity of the governing equations, most of these models have relied on commercial software for simulation. Additionally, in some models, constant properties are assumed, while in others, variable properties are considered to reflect more realistic operating conditions. Additionally, some articles consider radiation heat transfer in the channels, while others omit it. Given the relatively new nature of fuel cell technology and the absence of precise models and standardized performance characteristics, fuel cell modeling remains essential. A key difference between the current model and previous ones is the comprehensiveness of the heat transfer, fluid dynamics, and electrochemical models. Furthermore, unlike previous models, this study aims to investigate the SOFC in a real geometric configuration, specifically focusing on the channel design.

2 Modeling

The complexity of SOFC modeling, particularly due to the interdependence of the governing equations (especially when properties are variable), requires high-performance computing to solve the nonlinear, interdependent partial differential equations. Although computational technology has advanced, a code capable of solving multi-dimensional, interdependent equations would still be slow, if available. Moreover, models with such a high level of detail are not practical for applications such as fuel cell stack modeling. To reduce computational time and eliminate unnecessary complexities, the following assumptions have been made in this modeling:

- A medium-temperature planar-type fuel cell with co-directional current and anode support is considered.
- The flow in fuel and air channels is one-dimensional (along the channel), fully developed, and non-isothermal.
- Mass diffusion along the fuel and air channels is neglected in comparison with convective.
- Due to the high electrical conductivity of the electrodes, the voltage drop in them is ignored.
- The fuel entering the anode channel includes

methane, hydrogen, water vapor, carbon monoxide, and carbon dioxide, and the oxidizer entering the cathode contains oxygen and nitrogen.

- Only hydrogen electrooxidation, methane steam-reforming and water-gas shift reactions are considered, the first reaction in the PEN and the next two reactions in the fuel channel. The rate of steam reforming reaction is considered as equilibrium.

2.1 Governing equations

The governing equations include conservation of mass, momentum, energy and Electrochemical relations. The conservation equations for the fuel and air channels, electrodes and electrolyte, and fuel and air distributor plates are derived in reference [3] and are summarized in Table 1.

Table 1. Governing equations in different regions.

Equation - Region	Governing equations
Continuity - Fuel channel	$\frac{\partial C_{i-f}}{\partial t} + \frac{\partial(u_f C_{i-f})}{\partial x} = -\frac{\dot{C}_{i-f}''}{H_{fc}} \quad (3)$
Momentum - Fuel channel	$\rho_f \frac{\partial u_f}{\partial t} + \rho_f u_f \frac{\partial u_f}{\partial x} = -\frac{\partial p_f}{\partial x} + \frac{4}{3} \frac{\partial}{\partial x} \left(\mu_f \frac{\partial u_f}{\partial x} \right) - 2f_{fc} \frac{\mu_f u_f}{D_{H-fc}^2} \quad (4)$
Energy - Fuel channel	$\begin{aligned} & \rho_f \frac{\partial(C_{v-f} T_f)}{\partial t} + \rho_f u_f \frac{\partial(C_{v-f} T_f)}{\partial x} \\ & = \frac{1}{H_{fc}} \left[\dot{\rho} \Delta h + h_f(T_s - T_f) + h_f(T_i - T_f) \frac{W_c + 2H_{fc}}{W_c} - \frac{\dot{\rho}'' p_f}{\rho_f} \right] \\ & - p_f \frac{\partial u_f}{\partial x} + \frac{4}{3} \mu_f \left(\frac{\partial u_f}{\partial x} \right)^2 \end{aligned} \quad (5)$
Energy - PEN	$\begin{aligned} & \rho_s C_s \frac{\partial T_s}{\partial t} = k_s \frac{\partial^2 T_s}{\partial x^2} \\ & + \frac{1}{W_c H_s} \left[-h_f(T_s - T_f) W_c - h_a(T_s - T_a) W_c - \frac{2\sigma(T_s^4 - T_i^4) W_c}{\frac{1}{\epsilon_s} + \frac{(1-\epsilon_i) W_c}{\epsilon_i(W_c + H_f + H_a)}} \right. \\ & \left. - P_e'' W_c' + \dot{\rho}_f'' (h_{fuel} + h_{air} - h_{products}) W_c \right] \end{aligned} \quad (6)$
Energy - Fuel and oxidant distributor	$\begin{aligned} & \rho_i C_i \frac{\partial T_i}{\partial t} = k_i \frac{\partial^2 T_i}{\partial x^2} \\ & + \frac{1}{W_c H_i' + W_i H_i} \left[-h_f(T_i - T_f)(W_c + 2H_f) - h_a(T_i - T_a)(W_c + 2H_a) \right. \\ & \left. + \frac{2\sigma(T_s^4 - T_i^4) W_c}{\frac{1}{\epsilon_s} + \frac{(1-\epsilon_i) W_c}{\epsilon_i(W_c + H_f + H_a)}} \right] \end{aligned} \quad (7)$

In the Equation (4), p_f is the static pressure of the fuel in the channel, μ_f is the dynamic viscosity of the fuel mixture, and D_{H-fc} is the hydraulic diameter of the fuel channel. Also, f_{fc} is Fanning's coefficient of friction, which is a constant value and a function of the aspect ratio of the channel for the fully developed laminar flow in the square channel. For both fuel and air channels, the aspect ratio is $H_{fc}/W_c = 1/3$, so the value of $f_{fc} = 17.06$. The movement equation in the air channel is similar to that of the fuel channel.

In the Equation (5), C_{v-f} is the specific heat capacity at constant volume of the gas mixture, T_f is the temperature of the gas mixture, T_s is the temperature of the PEN section, and T_i is the temperature of the

fuel distributor plate (or bipolar plate in the fuel cell stack). Also, $\dot{\rho}''$ and Δh represent the reaction rate of fuel modification (heater reformation and water-gas shift reaction) per unit of channel-electrode interface and reaction enthalpy, respectively. h_f is the convective heat transfer coefficient in the fuel channel, which is expressed by the relation $h_f = Nu_{fc} k_f / D_{H-fc}$. In this relation, D_{H-fc} is the hydraulic diameter of the channel, k_f is the thermal conductivity of the fuel and Nu_{fc} is the Nusselt number of the fuel channel, which is a constant value assuming the uniformity of the ambient temperature distribution in the channel and is a function of the aspect ratio of the channel. For the air and fuel channel with an aspect ratio of 1/3, the

Nusselt number is $Nu_{fc} = 3.95$.

The anode, electrolyte, and cathode are considered as a single part (PEN). The Equation (6) states that the temporal and spatial temperature changes in PEN are caused by heat transfer due to convective, radiation, electrical work to transfer electrons and ions, electrochemical reactions, and heat flux due to the entry and exit of fuel and oxidizer into the channels. $\rho_s = 5900 \text{ kg/m}^3$, $C_s = 0.5 \text{ kJ/kg} \cdot \text{K}$ and $k_s = 2 \text{ W/m} \cdot \text{K}$ respectively for the density, specific heat capacity, and thermal conductivity of PEN, $\epsilon_s = 0.8$, and $\epsilon_i = 0.1$ respectively for the emission coefficient of PEN and distributor plate [7]. σ is the Stefan-Maxwell constant and h is the enthalpy of different fluxes of fuel, oxidizer, and reaction products. To evaluate the radiation heat transfer, the radiation heat transfer relation in a two-surface chamber and the assumption of gray surface have been used. Also, P_e'' is the surface density of electric power produced by the fuel cell, which is equal to $P_e'' = Vj$, where V is the fuel cell voltage and j is the current density.

The fuel distributor and oxidizer plates are non-porous and are responsible for distributing the reactants on the electrodes and removing the reaction products, heat, and electricity in the fuel cell. The Equation (7) states that the spatial and temporal temperature changes in the fuel and air distributor plate (bipolar plate in the fuel cell stack) are caused by convective heat transfer, and radiation. Assuming that the properties of these plate are constant, $\rho_i = 8000 \text{ kg/m}^3$, $C_s = 0.5 \text{ kJ/kg} \cdot \text{K}$ and $k_s = 25 \text{ W/m} \cdot \text{K}$ are respectively density, specific heat capacity, and thermal conductivity. The electrochemical equations are given in reference [2].

2.2 Simplification of thermophysical properties and governing equations

In order to reduce the calculation time and increase the stability of the model under different working conditions, reasonable simplifications have been made to the thermophysical properties and governing equations. First, the temperature dependence of the thermophysical quantities in the model is investigated. Then, the terms in the governing equations are compared in terms of their order, and terms of lower order are removed. To ensure the accuracy of the simplifications, the results before and after simplification are presented and compared.

Thermophysical properties. The thermophysical properties of each species, ϕ , are expressed in the model

as a function of temperature as follows:

$$\phi = a_0 \left[a_1 \left(\frac{T}{1000} \right) + a_2 \right]. \quad (8)$$

In this relation, a_0 is a unit conversion coefficient, a_1 and a_2 are coefficients based on the curve fitting of the property ϕ as a function of temperature in the range of 600-1000 K, and T is the temperature in Kelvin.

In order to check how each property changes with respect to temperature, the quantity S is defined as follows:

$$S = \frac{1}{\phi} \frac{d\phi}{dT} = \frac{a_1}{a_1 T + 1000 a_2}. \quad (9)$$

Thus, the quantity S represents the relative change of each property with respect to temperature in the operating range of the fuel cell. Table 2 shows the maximum value of each thermophysical quantity.

Table 2. Maximum dependence of thermophysical quantities on temperature.

Thermophysical properties	The value of changes, S (%/K)	The species with the most changes
Gibbs free energy, G	0.11	H ₂
Enthalpy, H	-0.17	CH ₄
Specific heat capacity, C_P	0.07	CH ₄
Thermal conductivity, K	0.13	H ₂ O(v)
Viscosity, μ	0.11	H ₂ O(v)

According to the values in Table 2, it can be observed that the average value of changes of each quantity in an interval of 100 K is less than 20%. Therefore, it can be assumed that the value of these quantities is independent of the axial temperature distribution. However, the governing equations have been investigated in two cases: one where the properties depend on temperature and one where the properties are assumed to be temperature-independent, and their results have been compared.

In the case of temperature-dependent properties, the value of each quantity at each point is calculated based on the temperature at that point. In contrast, for temperature-independent properties, the value of each quantity is calculated using the inlet temperature to the fuel cell. As a result, the properties along the length of the fuel cell channel are assumed to be constant. Additionally, other quantities that are directly related to these thermophysical properties have also been compared.

In Figure 2, the change in specific heat capacity is compared between the fuel and air channels. As can be

seen, the deviation is insignificant. Similarly, in Figures 3 and 4, the changes in thermal conductivity and dynamic viscosity for the fuel and air mixtures in both channels are compared. To investigate the dependence of Gibbs free energy on temperature, the open circuit voltage of the cell (Figure 5) is used, which shows a small error.

Table 3. The influence of constant thermophysical properties on fuel cell working parameters.

Quantity	Value	Percentage of change
Power of fuel cell	7.366 W	0.84%
Efficiency of the first law	47.96%	0.82%
Efficiency of the second law	72.06%	-0.04%

Although some of the fuel and oxidizer properties (such as viscosity) change slightly along the fuel cell channels, as indicated by the values in Table 2, the assumption of constant thermophysical properties along the channels has little impact on the operating parameters of the fuel cell. However, an important advantage of assuming constant properties is that it reduces the computation time by 16.7%.

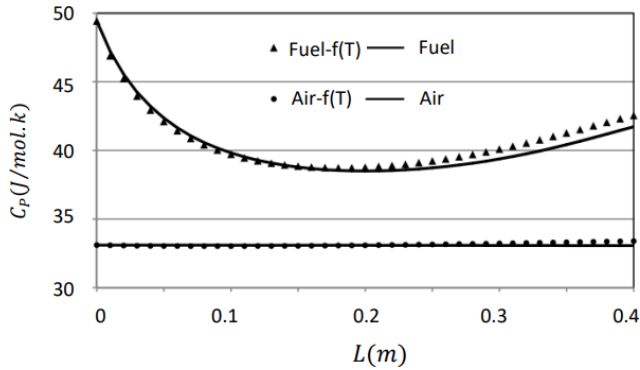


Fig. 2. Comparison of specific heat capacity in fuel and air channels in two states of dependence and non-dependence on temperature.

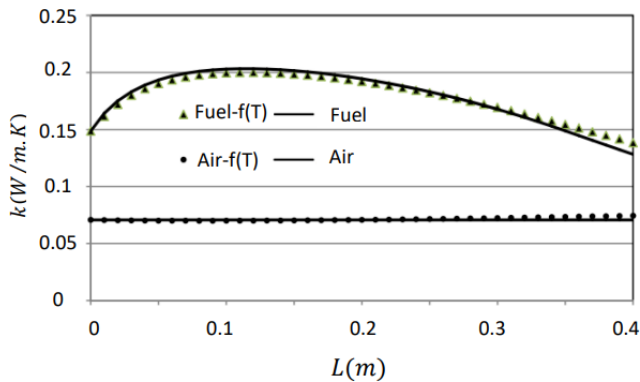


Fig. 3. Comparison of thermal conductivity in fuel and air channels in two states of dependence and non-dependence on temperature.

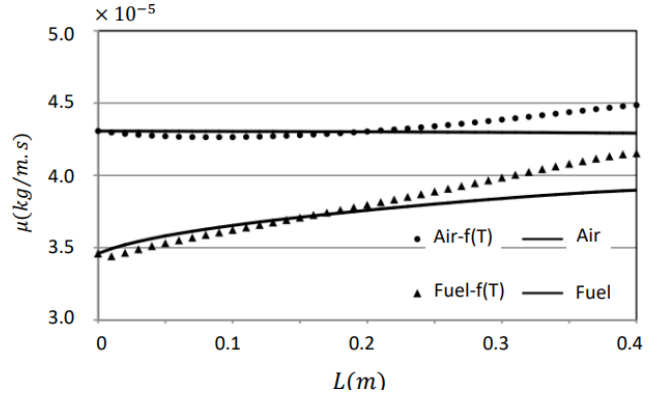


Fig. 4. Comparison of dynamic viscosity in fuel and air channels in two states of dependence and non-dependence on temperature.

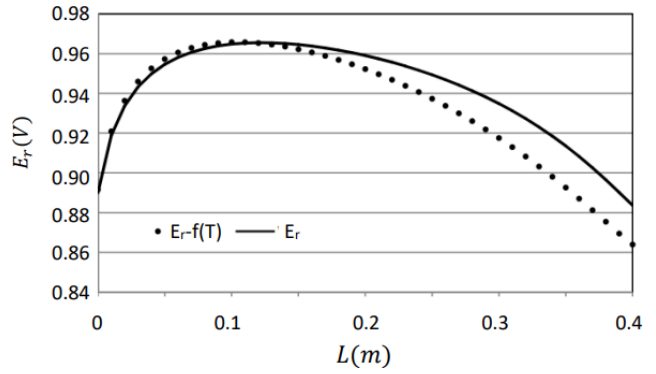


Fig. 5. Comparison of open circuit voltage in two states of dependence and non-dependence on temperature.

Governing equations. To simplify the governing equations, the order of each term in the equation should first be compared with that of the other terms in the equation. Based on the order of each term, a decision can then be made about whether to remove it. In the mass conservation equation for the fuel channel, excluding any of the terms (other than the time term, $\partial/\partial t$) would eliminate the effect of a dominant phenomenon. Therefore, none of the terms in this equation can be removed. This also holds true for the mass conservation equation in the air channel.

$$\frac{\partial C_{i-f}}{\partial t} + \frac{\partial(u_f C_{i-f})}{\partial x} = -\frac{\dot{C}''_{i-f}}{H_{fc}} \quad (10)$$

In the momentum conservation equation for the fuel channel, the order of each term is shown in Figure 6. As seen, the order of the fourth term (axial friction) is lower than the others and can be removed. The next lowest order corresponds to the second term (momentum displacement), followed by the third term (pressure gradient) and the fifth term (wall friction), which

are of the same order. Therefore, it can be concluded that in the fuel channel, the pressure gradient and wall friction are balanced. The relative stability of the velocity along the channel is one reason for the low order of the second and fourth terms. According to Figure 7, this conclusion also holds for the air channel.

$$\underbrace{\rho_f \frac{\partial u_f}{\partial t}}_1 + \underbrace{\rho_f u_f \frac{\partial u_f}{\partial x}}_2 = - \underbrace{\frac{\partial p_f}{\partial x}}_3 + \underbrace{\frac{4}{3} \frac{\partial}{\partial x} \left(\mu_f \frac{\partial u_f}{\partial x} \right)}_4 - \underbrace{2f_{fc} \frac{\mu_f u_f}{D_{H-fc}^2}}_5 \quad (11)$$

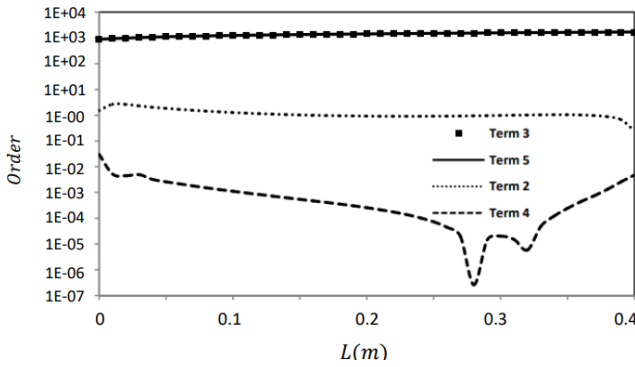


Fig. 6. The order of the sentences in the momentum conservation equation in the fuel channel.

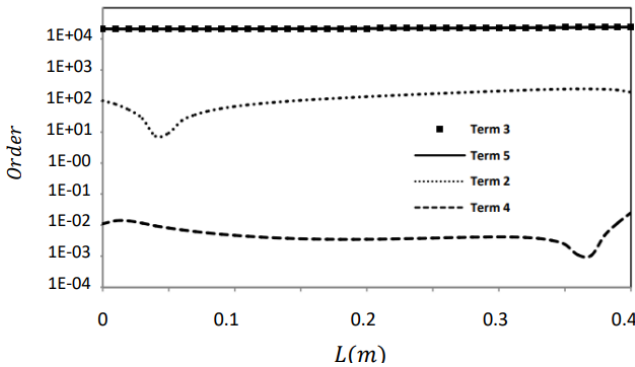


Fig. 7. The order of the sentences in the momentum conservation equation in the air channel.

Therefore, it is expected that removing terms with a low order will have little effect on the accuracy of the model. As before, for a quantitative comparison, the fuel cell's production power, energy efficiency, and voltage efficiency – its main operating quantities – have been compared in the two mentioned states. The results of this comparison are presented in Tables 2 to 4. As shown, removing the low-order terms did not alter the fuel cell's operating quantities but did reduce the

calculation time. Additionally, the order of terms in the energy conservation equation for the fuel channel is shown in Figure 8.

$$\underbrace{\rho_f \frac{\partial(C_{v-f}T_f)}{\partial t}}_1 + \underbrace{\rho_f u_f \frac{\partial(C_{v-f}T_f)}{\partial x}}_2 = \frac{1}{H_{fc}} \left[\underbrace{\dot{\rho}'' \Delta h}_3 + \underbrace{h_f(T_s - T_f)}_4 + \underbrace{h_f(T_i - T_f) \frac{W_c + 2H_{fc}}{W_c}}_5 - \underbrace{\frac{\dot{\rho}'' p_f}{\rho_f}}_6 \right] - \underbrace{p_f \frac{\partial u_f}{\partial x}}_7 + \underbrace{\frac{4}{3} \mu_f \left(\frac{\partial u_f}{\partial x} \right)}_8 \quad (12)$$

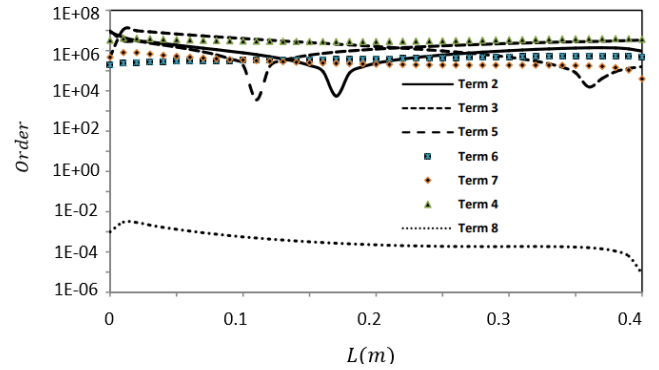


Fig. 8. The order of the sentences in the energy conservation equation in the fuel channel.

Table 4. The effect of removing low-order sentences from the governing equations on fuel cell working parameters.

Quantity	Value	Percentage of change
Power of fuel cell	7.366 W	0.0%
Efficiency of the first law	47.96%	0.0%
Efficiency of the second law	72.06%	0.0%

2.3 Non-dependence of the solution on the number of grid points

Typically, increasing the number of grid points improves the accuracy of the solution, but it also significantly increases the computational cost. Therefore, it is essential to find the optimal grid that strikes a balance between calculation accuracy and computational cost. Since no strong gradients are expected in the solution domain of this model, a uniform grid was used. This was further investigated by selecting a non-uniform grid at the entrance of the cell, where the highest gradients of the quantities were anticipated. The present model was investigated using the input parameters listed in Table 5. The dependence of the solution on the number of network nodes was examined

by using networks with 5, 10, 20, 40, and 80 nodes. The changes in current density, temperature, and molar concentration of hydrogen were analyzed for each number of nodes. The curves for mass fraction and current density are shown in Figures 9 and 10. As seen in the figures, as the number of nodes increases along the domain, the changes become progressively smaller. For the 80-node case, the results were virtually identical to those for the 40-node case. Therefore, 40 nodes were chosen for the grid to extract the final results.

Table 5. Input parameters of the model [8, 9].

Fuel consumption coefficient, U_f	75%
Amount of additional air, λ_a	8.5
Inlet fuel temperature, T_f^0	1023 K
Inlet air temperature, T_a^0	1023 K
Inlet fuel pressure, P_f^0	1 bar
Inlet air pressure, P_a^0	1 bar
Average current density, j_{av}	5000 A/m ³
Molar percentage of input fuel species, (with 10% fuel reforming in the ratio of [air/carbon] = 2)	CH ₄ 28.1%, H ₂ 12.0%, H ₂ O 56.7%, CO 0.5%, CO ₂ 2.7%
Molar percentage of input air species	O ₂ 21%, N ₂ 79%

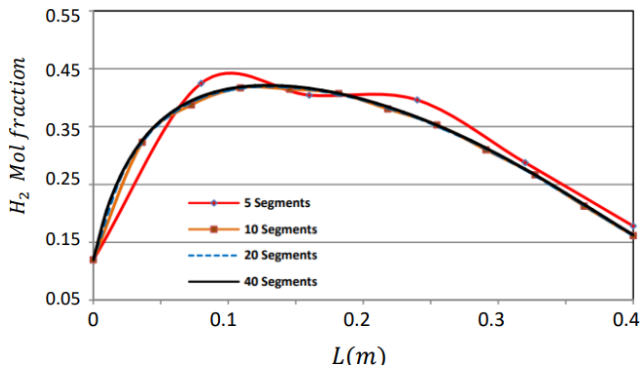


Fig. 9. Dependence of molar concentration of hydrogen on the number of grid points.

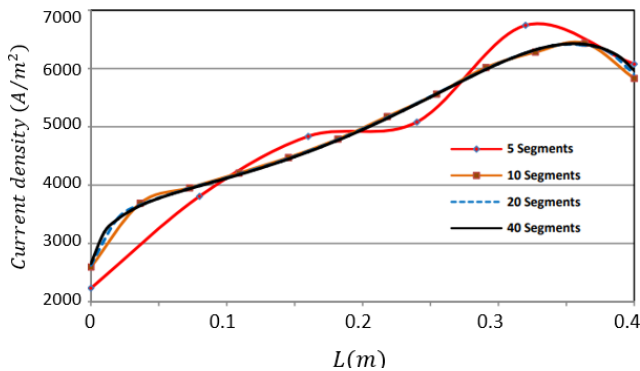


Fig. 10. Dependence of current density distribution on the number of grid points.

2.4 Validation

Several studies have been carried out on solid oxide fuel cell modeling, but validation with experimental data has been rare. Due to the lack of available experimental data, the model validation was performed using the modeling results of Iora et al. [9]. In Figure 11, the mole fraction of the species in the fuel channel (including methane, hydrogen, and water vapor) is compared with the results of Ayora et al., with the maximum error being less than 1%.

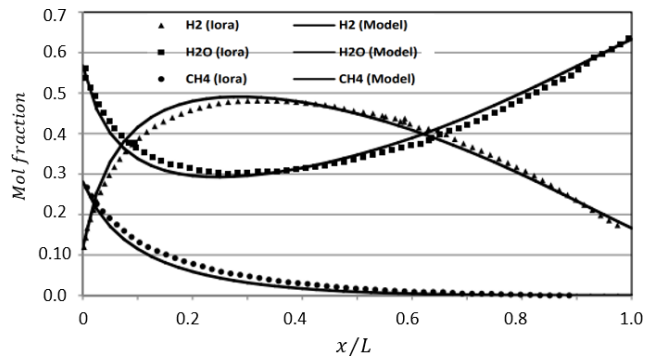


Fig. 11. Distribution of the mole fraction of methane, hydrogen and water vapor species in the fuel channel and their comparison with the values of Iora et al. [9].

In Figure 12, the dimensionless velocity curve along the fuel and air channels is presented. This curve shows good accuracy compared to Iora's model, with maximum errors of 3% and 1% for the fuel and air channels, respectively. The dimensionless velocity is defined as the ratio of the velocity at each section to the channel inlet velocity. A similar comparison was made for the dimensionless pressure, with the maximum error in both the fuel and air channels being less than 1%. However, due to the limited space in the article, this comparison is not included.

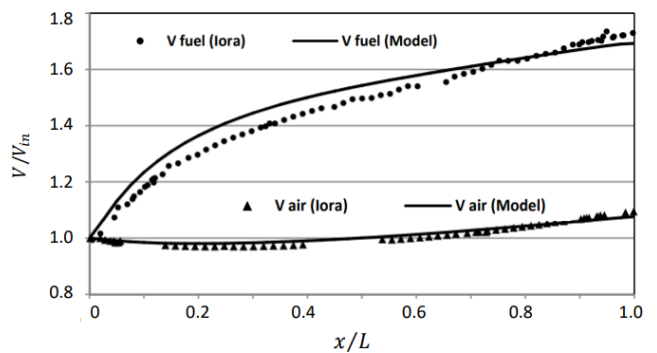


Fig. 12. Dimensionless velocity distribution in fuel and air channels and its comparison with the values of Iora et al. [9].

3 Results and Discussion

In this section, the results of the model are first examined under the reference conditions, followed by a parametric analysis based on the key working parameters. The results are obtained using the input conditions listed in Table 5, along with the simplifications made in the properties and equations.

Figure 13 shows the molar concentration distribution of species in the fuel channel, illustrating the effect of simultaneous fuel reforming and hydrogen oxidation reactions. Due to the high methane concentration at the inlet of the cell, the rate of the reforming reaction increases significantly, leading to a rapid decrease in the concentrations of methane and water vapor, along with a sharp increase in the hydrogen concentration. After a significant portion of the incoming methane is consumed in the first 20% of the fuel channel's length, the hydrogen concentration increases sharply, and the rate of the reforming reaction decreases, with the oxidation reaction becoming dominant. As a result of the oxidation reaction, the hydrogen concentration gradually decreases while the water vapor concentration increases. Additionally, as the concentration of carbon monoxide rises due to the fuel reforming reaction, the rate of the shift reaction also increases, leading to a gradual rise in the carbon dioxide concentration.

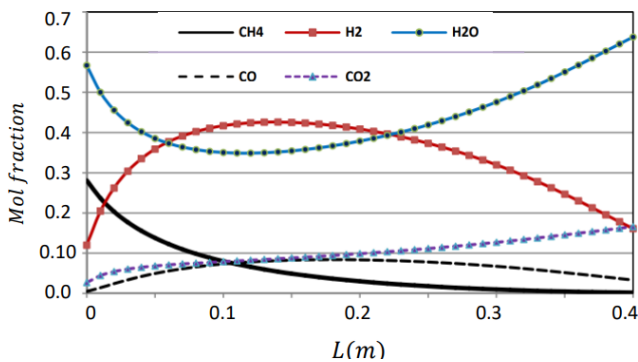


Fig. 13. Molar concentration distribution of species in the fuel channel.

Figures 14 and 15 shows the effect of increasing the inlet temperature of fuel and air mixture on voltage and output power, as well as energy efficiency and temperature gradient in the PEN. As seen, the overall effect of this change is an increase in output power, voltage, and energy efficiency. Additionally, increasing the inlet temperature leads to a decrease in the temperature gradient within the fuel cell, although this effect reverses after reaching the minimum temperature gradient point.

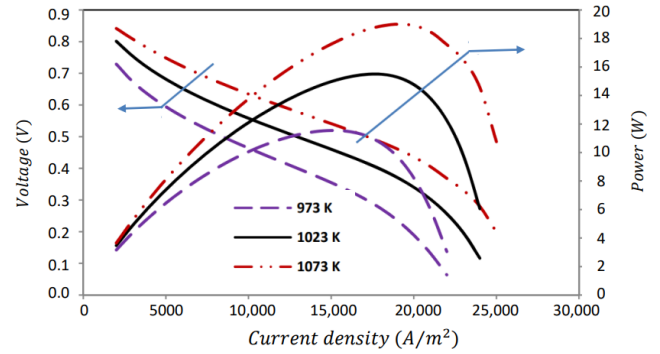


Fig. 14. The effect of changing the input temperature on the output power and voltage of the fuel cell.

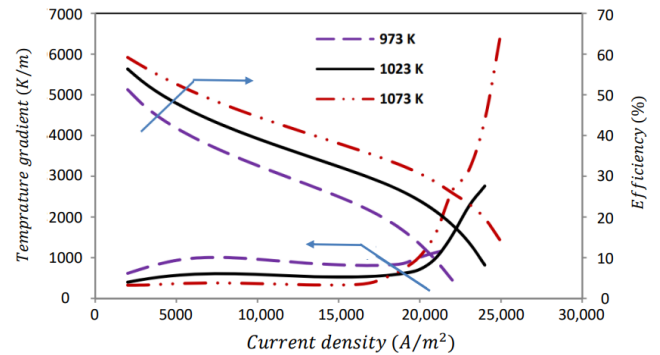


Fig. 15. The effect of inlet temperature variation on energy efficiency and maximum temperature gradient in PEN.

Figure 16 shows the effect of varying the fuel consumption coefficient on the voltage and output power of the fuel cell. As observed, with an increase in the current density of the fuel cell, the losses also increase, leading to a decrease in the output voltage. The output power initially increases due to the higher voltage, but it gradually decreases as the output voltage continues to decrease.

According to the figure, the power curve has a maximum point, and the operating point of the fuel cell is typically chosen to be close to this maximum power point. As the fuel consumption coefficient increases, the cell's current limit decreases, and the maximum power point shifts to a lower current density. The decrease in power and output voltage at higher fuel ratios is due to the reduced concentration of reactants within the fuel cell. At a current density lower than the maximum power point, changing the fuel consumption coefficient has no effect on the performance curve of the fuel cell, as the reactant concentration is sufficiently high. However, at a current density above the maximum power point, the decrease in reactant concentration becomes more pronounced, leading to a greater

difference in the power and voltage curves of the fuel cell.

Figures 17 and 18 show the effect of increasing the percentage of fuel pre-reforming on voltage, output power, energy efficiency, and the maximum temperature gradient in the PEN. The fuel pre-reforming percentage is defined as the fraction of methane that has been converted into hydrogen through the fuel reforming reaction in the external reformer. Increasing the amount of fuel pre-reformation reduces the methane content in the input fuel, leading to a decrease in the

rate of the reforming reaction. This reduction in the reforming reaction rate lowers its cooling effect, causing the fuel cell temperature to rise. The increase in power, output voltage, and energy efficiency is attributed to the higher fuel cell temperature. Additionally, the decrease in the reforming reaction rate leads to a reduction in the temperature gradient within the cell. Although this is the only parameter where all the effects of its increase are favorable for the fuel cell's performance, it results in higher costs for the external reforming equipment, raising the overall system cost.

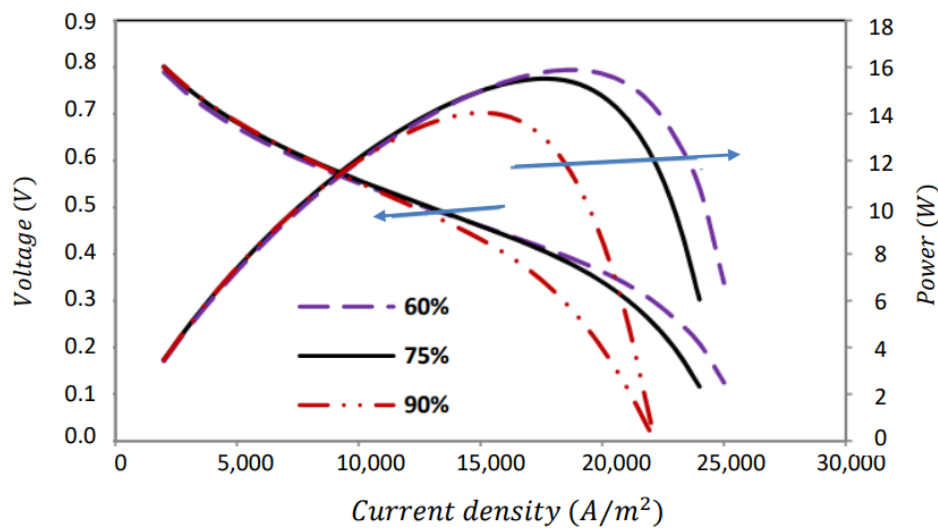


Fig. 16. The effect of variation of in the fuel consumption coefficient on output power and voltage.

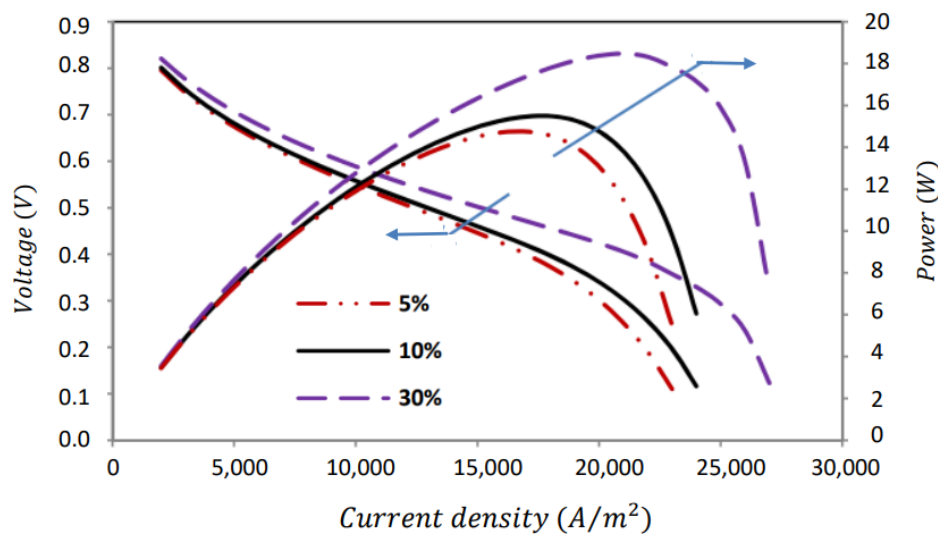


Fig. 17. The effect of changing the amount of fuel pre-reformation on the voltage and output power of fuel cell.

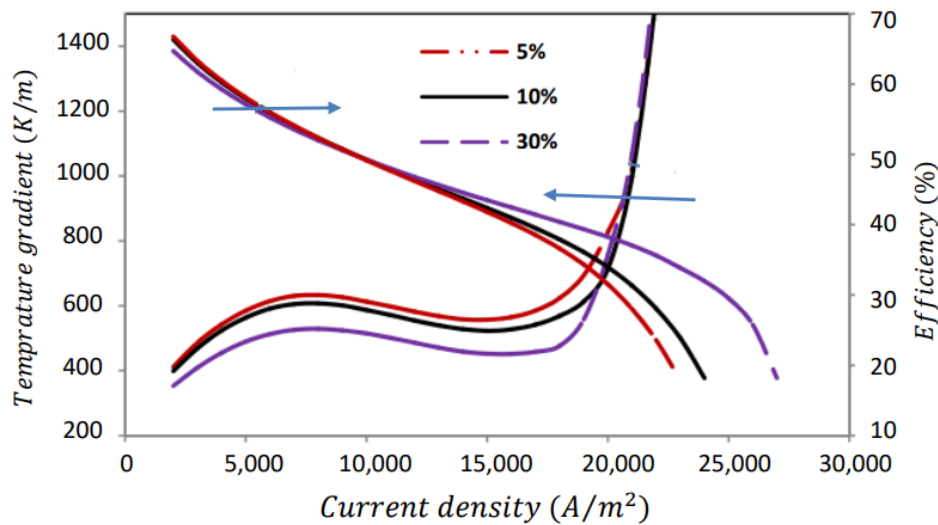


Fig. 18. The effect of changing the amount of fuel pre-reformation on energy efficiency and maximum temperature gradient in PEN.

4 Summary

SOFCs are important in the household and power plant sectors due to their high operating temperature range of 800-1000 degrees Celsius, versatility in fuel sources, low emissions of NO_x and SO_x pollutants compared to heat engines, resistance to sulfur, insensitivity to carbon monoxide (CO), and the lack of a need for catalysts. In this paper, a solid oxide fuel cell is modeled. The effect of temperature-dependent properties has been investigated, and it was found that their impact on the results was not significant. Therefore, to save program execution time, results were obtained using constant properties. Additionally, the effects of parameters such as the percentage of fuel pre-reforming and the temperature of the gases entering the fuel cell on its performance have been examined. The results show that the majority of the methane entering the fuel is consumed in the first 20% of the fuel channel. The high methane consumption at the fuel cell inlet increases the temperature gradient, and to prevent damage to the cell, this gradient should be kept at a low level. Additionally, a comparison of voltage losses revealed that cathodic and anodic activation losses, along with ohmic losses, are the dominant losses in the fuel cell.

References

- [1] Hajimolana SA, Hussain MA, Daud WAW, Soroush M, Shamiri A. Mathematical modeling of solid oxide fuel cells: A review. *Renewable and sustainable energy reviews*. 2011;15(4):1893–1917.
- [2] Hassanzadeh H, Farzad MA. Modeling and optimization of a single planar solid oxide fuel cell. *Modares Mechanical Engineering*. 2015;15(2):81–91.
- [3] Farzad MA. Modeling of a Combined Heat and Power Generation System based on Solid Oxide Fuel Cell and Photovoltaic in Residential Applications in Eastern Regions of IRAN; 2011. In Persian.
- [4] Tu B, Su X, Yin Y, Zhang F, Lv X, Cheng M. Methane conversion reactions over LaNi-YSZ and Ni-YSZ anodes of solid oxide fuel cell. *Fuel*. 2020;278:118273.
- [5] Lee TS, Chung J, Chen YC. Design and optimization of a combined fuel reforming and solid oxide fuel cell system with anode off-gas recycling. *Energy Conversion and Management*. 2011;52(10):3214–3226.
- [6] O'hayre R, Cha SW, Colella W, Prinz FB. *Fuel cell fundamentals*. John Wiley & Sons; 2016.
- [7] Aguiar P, Adjiman CS, Brandon NP. Anode-supported intermediate temperature direct internal reforming solid oxide fuel cell. I: model-based steady-state performance. *Journal of power sources*. 2004;138(1-2):120–136.
- [8] Aguiar P, Adjiman C, Brandon N. Anode-supported intermediate-temperature direct inter-

- nal reforming solid oxide fuel cell: II. Model-based dynamic performance and control. *Journal of Power Sources*. 2005;147(1-2):136–147.
- [9] Iora P, Aguiar P, Adjiman C, Brandon NP. Comparison of two IT DIR-SOFC models: Impact of variable thermodynamic, physical, and flow properties. Steady-state and dynamic analysis. *Chemical Engineering Science*. 2005;60(11):2963–2975.
- [10] Recknagle KP, Yokuda ST, Jarboe DT, Khaleel MA. Analysis of Percent On-Cell Reformation of Methane in SOFC Stacks: Thermal, Electrical and Stress Analysis. Pacific Northwest National Lab.(PNNL), Richland, WA (United States of America; 2006.
- [11] Petersen T, Houbak N, Elmegaard B. A zero-dimensional model of a 2nd generation planar SOFC using calibrated parameters. *International Journal of Thermodynamics*. 2006;9(4):147–159.
- [12] Cheddie DF, Munroe ND. A dynamic 1D model of a solid oxide fuel cell for real time simulation. *Journal of Power Sources*. 2007;171(2):634–643.
- [13] Xi H, Sun J, Tsourapas V. A control oriented low order dynamic model for planar SOFC using minimum Gibbs free energy method. *Journal of Power Sources*. 2007;165(1):253–266.
- [14] Chaisantikulwat A, Diaz-Goano C, Meadows ES. Dynamic modelling and control of planar anode-supported solid oxide fuel cell. *Computers & Chemical Engineering*. 2008;32(10):2365–2381.
- [15] Kang YW, Li J, Cao GY, Tu HY, Li J, Yang J. A reduced 1D dynamic model of a planar direct internal reforming solid oxide fuel cell for system research. *Journal of Power Sources*. 2009;188(1):170–176.
- [16] Salogni A, Colonna P. Modeling of solid oxide fuel cells for dynamic simulations of integrated systems. *Applied Thermal Engineering*. 2010;30(5):464–477.
- [17] Suther T, Fung A, Koksai M, Zabihian F. Macro level modeling of a tubular solid oxide fuel cell. *Sustainability*. 2010;2(11):3549–3560.
- [18] Vakouftsi E, Marnellos G, Athanasiou C, Couteirieris F. A detailed model for transport processes in a methane fed planar SOFC. *Chemical Engineering Research and Design*. 2011;89(2):224–229.
- [19] Zhu H, Kee RJ. A general mathematical model for analyzing the performance of fuel-cell membrane-electrode assemblies. *Journal of Power Sources*. 2003;117(1-2):61–74.
- [20] Kee RJ, Zhu H, Goodwin DG. Solid-oxide fuel cells with hydrocarbon fuels. *Proceedings of the Combustion Institute*. 2005;30(2):2379–2404.
- [21] Zabihian F, Fung A. A review on modeling of hybrid solid oxide fuel cell systems. *International journal of engineering*. 2009;3(2):85–119.
- [22] Modeling and Operation Assessment of a solid oxide fuel cell; 2006. 21th International Power Systems Conference.
- [23] Pirkandi J, Ghasemi M, Hamed M. Thermodynamic Performance Analysis of a Solid Oxide Fuel Cell and Micro Gas Turbine Hybrid Cycle in a CHP System. *FUEL AND COMBUSTION*. 2011;2:67–89. (In Persian).
- [24] Energy and exergy analysis of a gas turbine and sold oxide fuel cell hybrid system; 2010. (In Persian).
- [25] Bozorgmehri SH, Hamed M, Mohebi A H Ghobadzade, Aslannejad H. Operation and micro structure assessment of single cell of solid oxide fuel cell. *Energy*. 2011;2:21–36. (In Persian).
- [26] Kazemipoor P, Ommi FA. Modeling of a planar solid oxide fuel cell for combined heat and power systems. *Fuel and Combustion*. 2009;1:25–40. (In Persian).
- [27] Three-dimensional simulation of mass and energy transfer in the planar solid oxide fuel cell with counter flow; 2010. (In Persian).

Appendix A

Modeling of SOFC and solution of equations was done by Model Builder gPROMS 3.4.0 software in static mode. gPROMS is a software used to model industrial processes and used in the design, development, and optimization of equipment and processes. This software was prepared by the Process Engineering Center of the Royal College of England and has capabilities such as simulation, optimization, and parameter estimation in static and dynamic modes, which are very complex processes. This software is an equation-based modeling environment, which enables the user to enter the equations as they are on paper into the programming environment. This clarity and brevity of

language frees the user from focusing on numerical solution methods and focuses his attention more on the problem itself. In this software, equations are written based on the basic laws of chemistry, physics, and other governing laws. Then the aforementioned equations are converted into a partial algebraic-differential equation system and then solved with the help of advanced nu-

merical solvers. This software uses the LU factorization algorithm to solve linear algebraic equations, the Trigonometrical and Newton algorithms to solve non-linear algebraic equations, Rang-Kuta and finite difference algorithms for algebraic-differential equations, and simple and multiple shooting algorithms for Solving optimization problems is used.